The Astrophysical Journal, 831:154 (7pp), 2016 November 10 doi:10.3847/0004-637X/831/2/154

LOW-FREQUENCY RADIO OBSERVATIONS OF THE SOLAR CORONA WITH ARCMINUTE ANGULAR RESOLUTION: IMPLICATIONS FOR CORONAL TURBULENCE AND WEAK ENERGY RELEASES

V. Mugundhan[1], R. Ramesh[1], Indrajit V. Barve[1], C. Kathiravan[1], G. V. S. Gireesh[1], P. Kharb[1], and Apurva Misra[2]
[1] Indian Institute of Astrophysics, 2nd Block, Koramangala, Bangalore—560 034, Karnataka, India; mugundhan@iiap.res.in
[2] National Institute of Technology, Surathkal—575 025, Karnataka, India
Received 2016 June 2; revised 2016 August 25; accepted 2016 August 25; published 2016 November 4

ABSTRACT

We report on the first long baseline interferometer (length ≈8 km) observations of the solar corona at 37 MHz that were carried out recently with an angular resolution of ≈1′. The results indicate that, (1) discrete radio sources of the aforesaid angular size or even lesser are present in the solar corona from where radiation at the above frequency originates. This constrains the angular broadening of radio sources at low frequencies due to scattering by density turbulence in the solar corona; and (2) the observed sources in the present case correspond to the weakest energy releases in the solar atmosphere reported so far.

Key words: instrumentation: high angular resolution – instrumentation: interferometers – Sun: activity – Sun: corona – Sun: flares – Sun: radio radiation

1. INTRODUCTION

White-light observations of the solar corona during eclipses and with coronagraphs reveal structures of characteristic dimensions ∼10″ in the heliocentric distance (r) range of ≈1.1–2.0$R_\odot$ from where the low-frequency (100–30 MHz) radio radiation typically originates. This calls for radio observations in the above frequency range with high angular resolution, since there are unique advantages like: (1) simultaneous observations of both the corona overlying the solar disk as well as off the solar limb with the same instrument (see for example Kathiravan et al. 2002); (2) observations with good contrast even at short data integration times (≲100 ms); (3) sensitivity to density enhancements since radio brightness is $\propto n_e^2$, where n_e is the coronal electron density; (4) radio bursts associated with the solar transients are intrinsically more intense at low frequencies, since the associated emission processes (plasma/gyrosynchrotron mechanisms) are nonthermal in nature; and (5) simpler measurements of the coronal magnetic field through circular polarization observations (see for example Sasikumar Raja et al. 2014). Taking into consideration the minimal radio frequency interference (RFI) in Gauribidanur (Monstein et al. 2007; Kishore et al. 2015; Hariharan et al. 2016), the "stable" ionosphere during midday (Kassim et al. 2007), the proximity of the Sun's declination to the latitude of Gauribidanur (≈14°N) for a major part of the year, because of which the zenith angle-dependent ionospheric errors are expected to be smaller (Jacobson et al. 1991; Mercier & Chambe 2009), predicted small coronal radio source sizes (Subramanian & Cairns 2011), and the advancements in the field of digital signal processing, we thought a pilot study in the Gauribidanur observatory (Ramesh 2011a) with a simple radio interferometer that provides an angular resolution of ≈1′ could be useful. This is particularly so, since observations of the solar corona with high angular resolution at low frequencies is one of the key science targets for large interferometer arrays like the LOFAR, SKA, and the proposed expansion of the Gauribidanur RAdioheliograPH array (GRAPH).[3]

[3] www.iiap.res.in/centers/radio/array_expansion

2. OBSERVATIONS

The present work is the first of its kind at low frequencies (< 100 MHz), particularly in solar radio astronomy. So we have described the analog/digital receiver systems and the data processing techniques in detail in Appendices A–C. We used a simple cross-correlation-type radio interferometer for the present work, since the size of a radio source can be inferred from such observations. The setup has two stations. The primary receiving element in each station is a log periodic dipole antenna (LPDA; Kishore et al. 2014). Station 1 of the interferometer is one of the antenna groups in the Gauribidanur Radio Interferometric Polarimeter (Ramesh et al. 2008). It consists of sixteen LPDAs on an east–west line with a spacing of 10 m between the adjacent antennas (Figure 5). Station 2 consists of a single LPDA. The LPDAs in both the stations are oriented in the east–west direction. The width of the response pattern ("beam") of Stations 1 and 2 are ≈3° × 90° (Right Ascension (R.A.) × Declination (decl.)), and ≈60° × 90°, respectively. This indicates that their combined response (field of view, FOV) in the cross-correlation mode is ≈3° × 90°. The effective collecting area of Station 1 and Station 2 are ≈0.5λ^2 and ≈8λ^2, respectively, where λ is the wavelength corresponding to the frequency of observation. All the aforementioned LPDAs work has been designed for observations in the frequency range of ≈30–120 MHz with a voltage standing wave ratio (VSWR) of ≲2. The length (D) of the baseline between the two stations is ≈8 km in the east–west direction. In view of this long baseline, we call the setup a Long Baseline Interferometer (LBI). Its minimum detectable flux density at 37 MHz is ≈1500 Jy (1 Jy = 10^{-26} Wm^{-2} Hz^{-1}) for an observing bandwidth of ≈100 KHz and integration time of ≈50 ms. Note that the present antenna setup belongs to the category of rectangular or linear aperture with field only at the edges. In such a case, the half-power beam width is ≈29°λ/D (Kraus 1966). In the present case, $D \approx 8$ km and $\lambda = 8.1$ m. So the beamwidth is ≈1.′5.

During the first observing run with the LBI system in 2015 July, we carried out observations of Cygnus A (3C405) and the Sun at 37 MHz around their respective transits over the local meridian in Gauribidanur. Figure 1 shows the plot of the visibility amplitudes obtained from observations of Cygnus A

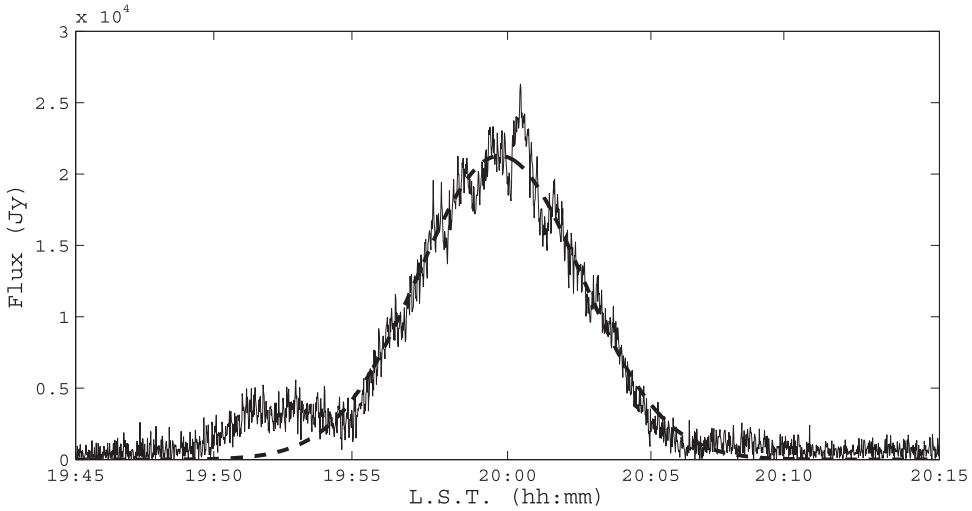

Figure 1. Visibility amplitudes obtained from observations of Cygnus A in the meridian transit mode with the LBI on 2015 July 10 at 37 MHz. The integration time used was ≈1 s. The "dotted" line is the fit to the observations. Its width corresponds to the FOV of the LBI along the R.A.

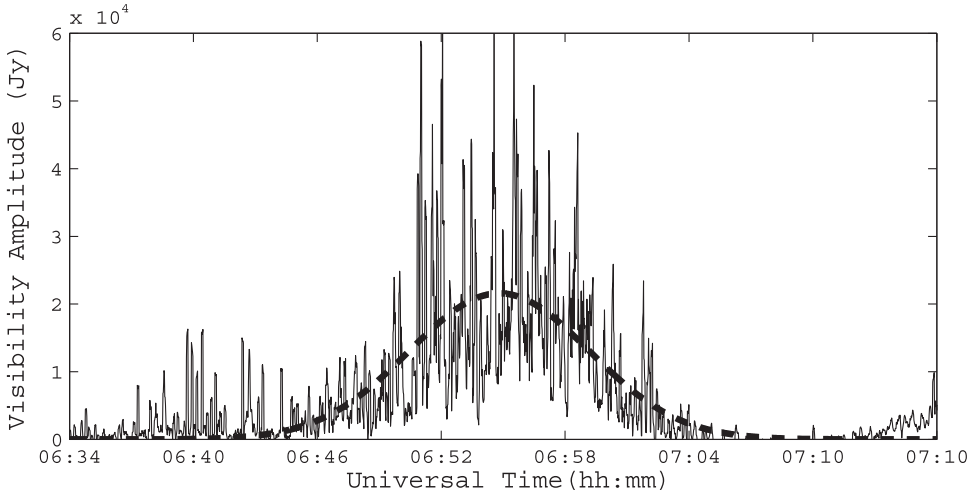

Figure 2. Same as Figure 1, but observations of noise storm bursts from the Sun on 2015 July 10.

on 2015 July 10. The R.A. and decl. of the source are $\approx 20^{h}00^{m}$ Local Sidereal Time and $\approx 40\overset{\circ}{.}7$, respectively. Its flux density (S) at 37 MHz (as reported from the total-power measurements) is ≈24,578 Jy (see for example Nelson 1985). But Cygnus A has an extent of $\approx 2'$, and the angular resolution of the LBI experiment in the present case is at 37 MHz is $\approx 1'$. This implies that the source should be marginally resolved (Kassim et al. 1996). From the calibrated UV-data available in the NRAO archive and assuming a spectral index of ≈ -0.7, we calculated the likely flux density of Cygnus A at the above angular resolution at 37 MHz to be $S \approx$ 21,273 Jy. Moving to solar observations with the LBI, we found that intense nonthermal radio emission from the Sun was observed with the GRAPH at 55 and 80 MHz during the period 2015 July 9–13. Similar emission was reported from observations elsewhere, also around the same time.[4] The long-lasting (~days) nature of the activity clearly indicates that it must be a noise storm source, since there are no other known sources of such radio emission from the Sun at low frequencies (Elgarøy 1977; Kai 1985; Ramesh et al. 2011b). Otherwise the Sun was "undisturbed" in 2015 July, particularly close to its transit time in Gauribidanur.[5] Since we had simultaneous observations with the LBI at 37 MHz during 2015 July 10–12, we present the same here. Figure 2 shows the plot of the visibility amplitudes obtained from the Sun on 2015 July 10 at 37 MHz in the meridian transit mode. The coordinates of the Sun on the above date were R.A. $\approx 06^{h}55^{m}$ universal Time (UT) and decl. $\approx 22\overset{\circ}{.}3$, respectively. We used Cygnus A observations to calibrate and convert the observed raw solar data to flux density values. There is clear evidence for correlated emission in the FOV of the LBI. Similar emission was observed on 2015 July 11 and 12. This indicates that discrete source radio sources of angular size $\lesssim 1'$ are present in the solar corona from where the 37 MHz radiation originates.

3. ANALYSIS AND RESULTS

The angular size of the noise storm continuum sources mentioned in the literature are $\approx 23'$ at 38.5 MHz (Kundu & Gopalswamy 1990). Such large-sized sources are expected to be completely resolved with observing instruments that have an

[4] ftp://ftp.swpc.noaa.gov/pub/warehouse/2015/2015_events/

[5] http://www.iiap.res.in/files/solarradioimages/gbd/H_July_2015.html

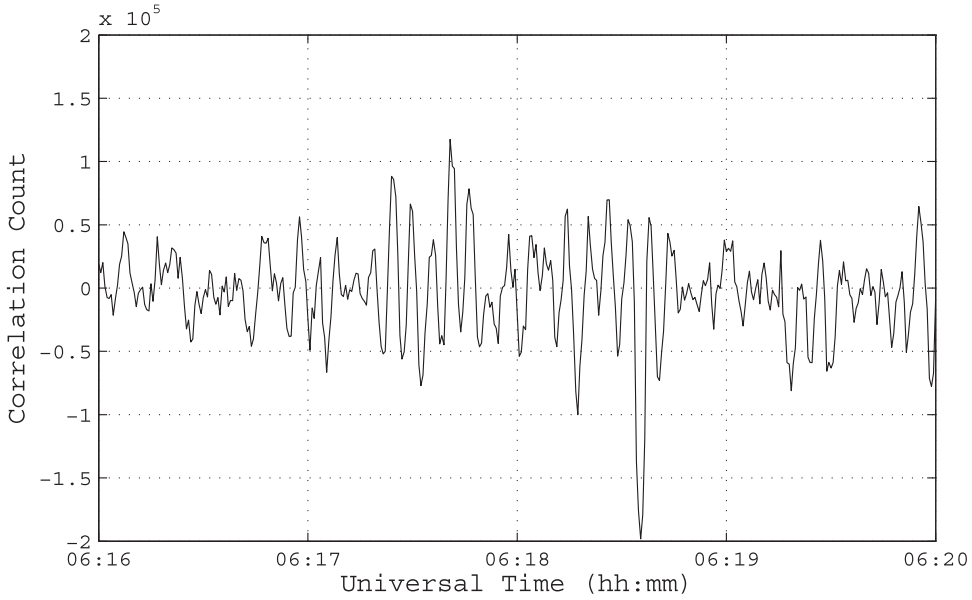

Figure 3. Interference fringes obtained with the LBI during the observations of a type III burst on 2015 August 9. The fringe width is $\approx 1'$.

angular resolution of $\approx 1'$ at 37 MHz, as in the present work. This implies that the LBI observations in Figure 2 correspond primarily to the noise storm bursts whose angular sizes are smaller than that of the continuum (Kai 1985). The present observations indicate that the sizes of the above bursts at 37 MHz are $\lesssim 1'$. Their peak flux densities are in the range $\approx$(0.5–6.0) $\times$ 10^4 Jy. Assuming circular symmetry for the source size, we find that the corresponding peak brightness temperatures (T_b) are $\approx$0.1–1.7 $\times$ 10^{10} K. These values are in reasonable agreement with the predicted T_b ($\approx 5 \times 10^{10}$ K) for strong noise storm bursts at 37 MHz (Thejappa 1991). We estimated the total flux density of the bursts in the present case from the auto-correlation of the signal received by Station 1 (i.e., the total power measured with zero baseline or spacing interferometer) in the LBI setup, and the value is $\approx 8.3 \times 10^4$ Jy. The contribution of the "background" solar corona to the above can be neglected, since it is expected to be comparatively very small at 37 MHz, $\approx 2 \times 10^3$ Jy (Erickson et al. 1977). These indicate that the flux density of the noise storm bursts observed with the LBI is $\approx$(0.06–0.72) times their total flux density. We also calculated the likely flux density of the background continuum at 37 MHz on 2015 July 10 using GRAPH observations at 55 and 80 MHz around the same epoch, and the value is $\approx 1.5 \times 10^4$ Jy. A comparison of this with the flux densities of the bursts at 37 MHz indicates that the latter are $\approx$(0.1–4) times the above value. Considering that the bursts are fluctuations of varying amplitude superimposed on the background continuum (Kai 1985), we find that at 37 MHz their flux densities are $\approx$(0.3–4) times above the flux density of the background continuum. Since the latter is resolved in the present LBI observations, we are able to notice even the bursts with small amplitude. The aforementioned range of flux densities of the bursts with respect to the background continuum are consistent with the results reported in the literature (see for example Malik & Mercier 1996; Mercier & Trottet 1997).

Observations with the LBI during a type III burst on 2015 August 9 indicate that it has a structure with an angular size of $\lesssim 1'$ at 37 MHz (see Figure 3). The calibrated peak flux density of the burst is $\approx$2000 Jy. This is about 4% of the total flux density ($\approx 4.8 \times 10^4$ Jy) observed at the same epoch with Station 1 of the LBI as mentioned above. The above values are in the range of flux densities of weak type III-like micro bursts at 38 MHz reported in the literature (Subramanian et al. 1993). The peak T_b of the type III burst observed with the LBI, estimated assuming circular symmetry for the source size as in the noise storm burst case, is $\approx 5.6 \times 10^8$ K. Since the lifetimes of type III bursts are limited ($\lesssim$25 s at a frequency like 37 MHz (Suzuki et al. 1985)), we speculate that the interference fringes in Figure 3 between $\approx$06:17–06:18 UT and $\approx$06:18–06:19 UT could also be attributed to successive emission from two spatially separated type III burst sources that were active at corresponding epochs.

Figure 4 shows the distribution of the noise storm bursts in Figure 2 with respect to their peak flux densities. An integration time of $\approx$50 ms was used to minimize the possible averaging of different individual bursts with short lifetimes. The fit to the distribution indicates that the latter follows a power-law pattern with an index (γ) of ≈ -2.5. The power-law indices of the fit to the distribution of the noise storm bursts observed on 2015 July 11 and 12 are also nearly the same. The average value of γ for the above three days is ≈ -2.4. Note that we used the generalized Pareto function for the present work, since it provides good fit to the extremes of the distribution (Arnold 2015). Considering that noise storm bursts are signatures of nonthermal processes involving small coronal magnetic energy releases (Benz 1995), the above results are consistent with the prediction that the power-law index for the distribution of weak energy releases in the solar atmosphere should be < -2 (Hudson 1991). We calculated the energy of the burst source using the relation (Elgarøy 1977),

$$W = S\delta t \delta \nu R^2 \Omega e^{\tau}, \quad (1)$$

where δt is the duration of the burst, ν is the observing frequency, $\delta\nu$ is the bandwidth of the burst, $R \approx 150 \times 10^9$ m is the Sun–Earth distance, Ω is the solid angle into which the radio waves are emitted, and τ is the optical depth. In the

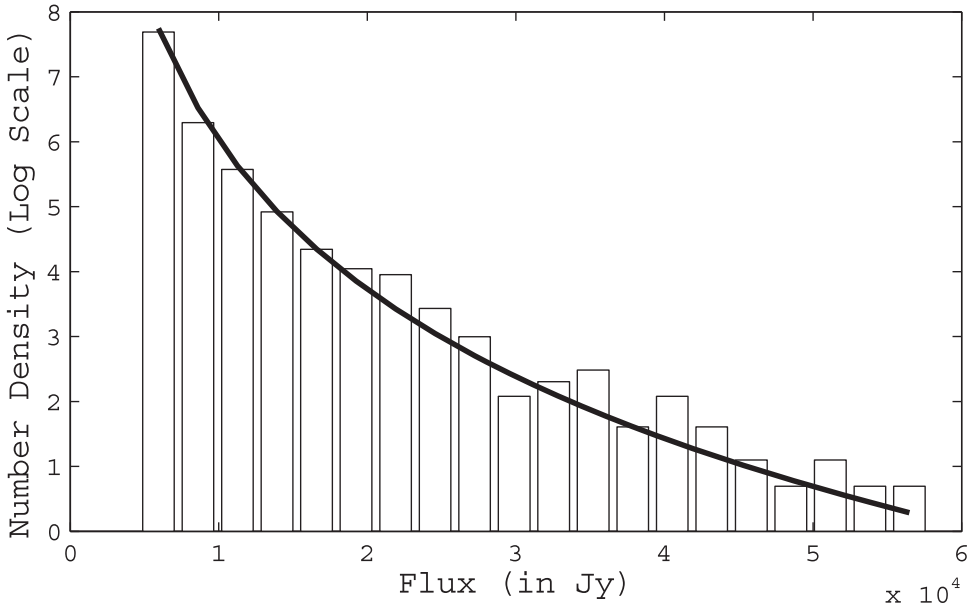

Figure 4. Distribution of the number of noise storm bursts observed on 2015 July 10 with respect to their peak flux densities. The "thick" black line is the fit to the distribution with a power-law index of ≈−2.5.

present case: $S \approx (0.5\text{–}6.0) \times 10^4$ Jy, $\delta t \approx 50$ ms, and $\nu = 37$ MHz. Assuming $\delta\nu = 0.02\nu \approx 0.7 \times 10^6$ Hz (Benz & Wentzel 1981), $\Omega \approx 0.15$ steradians (Steinberg et al. 1974), and $\tau \approx 1$ at 37 MHz (Ramesh 2005), we get $W \approx 6.4 \times 10^{16}$–$1.7 \times 10^{18}$ erg for the noise storm bursts in Figure 2. Note that the above value was obtained by assuming an efficiency (η) of $\approx 10^{-6}$ for the noise storm emission process, which starts with the acceleration of the associated nonthermal electrons (Elgarøy 1977). If we assume $\eta \approx 10^{-10}$ (Subramanian & Becker 2004), then $W \approx 6.4 \times 10^{20}$–$1.7 \times 10^{22}$ erg. Either way, these are by far the weakest energy releases in the solar atmosphere ever reported observationally (Porter et al. 1995; Mercier & Trottet 1997; Krucker & Benz 1998; Parnell & Jupp 2000; Ramesh et al. 2010). This indicates that observations with short integration times and high angular resolution (which fully resolves the "background" corona as well as the noise storm continuum), as in the present case, are important to unambiguously observe the aforementioned weak energy releases. Note that in the presence of the noise storm continuum, the term S in Equation (1) can be $\sim 10^6$ Jy at low frequencies (Nelson 1985). Obviously W will be correspondingly higher.

4. SUMMARY AND SCOPE

The LBI observations reported in the present work at 37 MHz clearly indicate that there are discrete radio sources with angular sizes $\lesssim 1'$ in the solar corona, and these correspond to the weakest energy releases there. In view of the possible contribution of the latter to the coronal energy budget (see for example Ramesh et al. 2013 and the references therein), similar observations, but preferably with an array of antennas in the two-dimensional imaging mode, are suggested. Such observations will also be helpful to localize the radio transients with respect to the associated coronal structures observed in other frequency bands of the electromagnetic spectrum (see for example Ramesh et al. 2012a).

Regarding scattering, the extent to which it broadens the angular size of the "undisturbed" Sun (Sastry 1994; Ramesh 2000; Ramesh et al. 2006) and/or a discrete source (Kerdraon 1979; Ramesh et al. 1999, 2012b; Ramesh & Ebenezer 2001; Kathiravan et al. 2011) at low radio frequencies is, to date, not clear. The present work indicates that if observations are carried out with appropriate angular resolution, discrete sources of sizes $\lesssim 1'$ could be observed even in the range $r \approx 1.5$–$2.0\ R_\odot$ from where the radio radiation at low frequencies like 37 MHz typically originate. This is consistent with the observations of discrete solar radio sources of angular sizes $\approx 31''$–$35''$ in the range $r \approx 1.20$–$1.25\ R_\odot$ reported recently by Mercier et al. (2015). These results constrain the angular broadening of radio sources at low frequencies due to scattering by density turbulence in the solar corona (Bastian 2004).

We thank the staff of the Gauribidanur observatory for their help in the fabrication, installation, and maintenance of the antenna/receiver systems, and the observations. We are grateful to N. Krishnan and his team in the Gravitation Laboratory, Tata Institute of Fundamental Research, Gauribidanur, for their kind consent to host Station 2 of the LBI interferometer in their premises, and their logistics support. I.M. van Bemmel, and Z. Paragi are acknowledged for their inputs related to VLBI observations. V.M. acknowledges K. Hariharan, H. Verkouter, and G. Tuccari for discussions. The Scientific Editors of the AAS are acknowledged for introducing us to Pareto distribution. We thank the referee for his/her kind comments, which helped us to present the results more clearly.

APPENDIX A
ANALOG FRONT-END RECEIVER

The RF signal from the individual antennas in Stations 1 and 2 pass through a high-pass filter (with 3 dB cut-off at $f_l = 25$ MHz), followed by a wideband amplifier with gain ≈28 dB, both located at the base of each antenna (see Figure 5). In the case of Station 2, the amplified signal from the

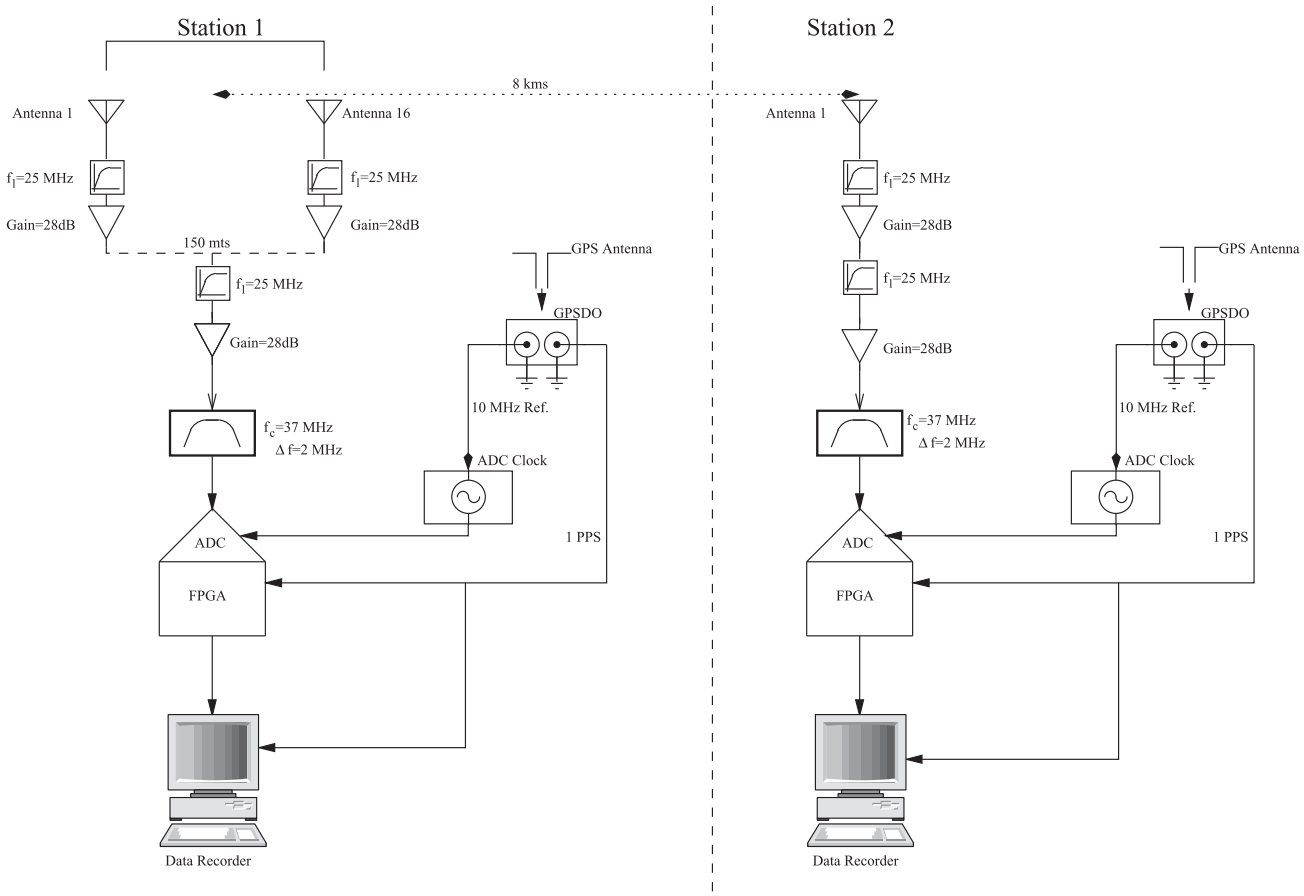

Figure 5. Block diagram of the antenna system and the receiver setup.

16 LPDAs are combined using amplitude and phase equalized RF coaxial cables, and a 16-way power combiner. The final output from Station 2 is further high-pass filtered and amplified, similar to the signal from the individual antennas in the station. Next, the RF signal from the two stations pass through bandpass filters with a center frequency (f_c) of 37 MHz and bandwidth $\Delta f \approx 2$ MHz. The output of the above filters is transmitted to independent data recording systems.

APPENDIX B
DIGITAL BACKEND RECEIVER

The data recording setup used in the present work is shown in Figure 6. AD9286, an 8-bit dual core analog-to-digital converter (ADC) with a maximum sampling rate of 500 million samples per second (MSPS) was used to digitize the input RF signal. The ADC has two clocking modes: simultaneous and interleaved. In the simultaneous mode, both the ADC cores sample the same data stream with the same sampling clock. The maximum sampling rate possible in this mode is 250 MSPS. In the interleaved mode, the data stream is sampled by both the cores, but the sampling clock in either core will be 180° out of phase with respect to the other. The ADC was used in the simultaneous mode for the present work. We used the most significant six bits in the ADC. The remaining two least significant bits in the ADC correspond to quantization noise, errors due to nonlinearity in the ADC, and background noise. By characterizing the ADC with sinusoidal inputs of different amplitudes we found that the signal-to-noise ratio (S/N) of the ADC is ≈36 dB, and the dynamic range is ≈40 dB. The above S/N agrees well with the expected value calculated using the relation $S/N = (6.02N + 1.76)$ dB, where N is the number of bits.[6] The dynamic range is sufficient to accommodate the ≈30–40 dB instantaneous variations in the solar radio flux during periods when the Sun is "active" (Nelson 1985). The use of six bits is also expected to be useful to identify the RFI in the observed data. Test results revealed that the performance of the ADC is optimal when the input signal level is ≈−20 dBm. Parameters like the DC offset, format of the output bits (2′s complement, offset binary etc.), and the clocking modes of the ADC can be set through a Serial Peripheral Interface (SPI). The ADC outputs the 8 bits and the sampling clock as parallel, Low Voltage Differential Signal (LVDS). A two-layer interface PCB (IPCB) was designed to transmit the parallel LVDS data to a Field Programmable Gate Array (FPGA) for packetization and further transmission. It is equipped with two ZPACK-HM-Zd-plus connectors to mate with the ADC board. The LVDS data from the ADC and the SPI control signals (between the FPGA and the ADC) are transmitted through the IPCB. 74HCT245 (a level shifter IC) for converting the 5V, 1 pulse per second (1PPS) signal from the Global Positioning System Disciplined Oscillator (GPSDO) module to an FPGA-compatible 3.3V signal is also included in the IPCB.

The FPGA used is a Virtex 5, XCV5LX110T chip, mounted on a XUPV5 Development Board. It has transceivers for high-speed differential communication and inbuilt cores for serial

[6] Analog Devices Tutorial MT-001.

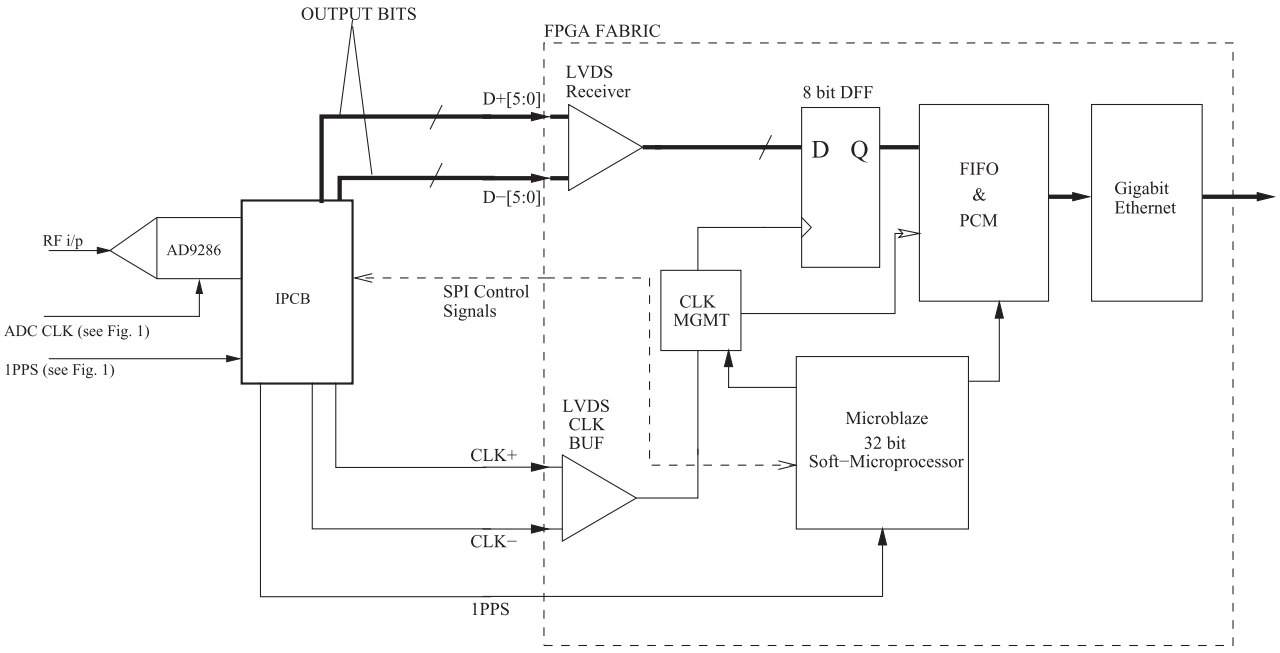

Figure 6. The data recording setup.

communication like ethernet, PCIe, Aroura, etc. The tasks of the FPGA in the present work are: (1) to capture the LVDS data from the ADC, (2) match the respective bits to form data bytes, (3) packetize the bytes suitable for communication through ethernet, (4) supply SPI control signals for the ADC, and (5) allow user interaction to set the start time and the duration of the observations. Gigabit ethernet communication was used to transmit the data to the computer. The SPI control of the ADC and user interaction are implemented on board FPGA using a Microblaze Soft-processor Core (SP). A Software Firmware was written in Embedded C for distribution of the SPI Control. The operation of the SP was synchronized to the 1PPS through programmable interrupts. The observation start time and duration are set using the 1PPS signal from the GPSDO (see Figure 5) as the reference. This helps in the synchronization of the entire operation to a common time and frequency reference.

The RF signal from the analog receiver is sampled at 64 MHz (ADC CLK). Further downsampling in cases where the RF signal bandwidth is <32 MHz can be done on board the FPGA. In the present case, the bandwidth is ≈ 2 MHz (see Figure 5). So the signal was downsampled by $\approx 16\times$ to reduce the data rate. The downsampling clock is synchronized to the sampling clock (64 MHz) using the Phase-Locked-Loop (PLL), which blocks in the FPGAs clock management (CLK MGMT) tiles. The 6 data bits from the ADC are concatenated with 2 extra bits. The 7th bit or the (MSB $-$ 1)th bit is a zero bit (always) and the 8th bit (the MSB) is the 1PPS signal of the GPSDO. This helps in distinguishing between the signal of interest and the time markers (1PPS signal), while aligning the time series data before cross-correlation. The bits are sampled in an 8-bit D-Flip Flop (DFF). The output of the DFF is written to an Asynchronous First-In-First-Out (FIFO). The latter has two separate clocks for read and write operations. The data write operation of the FIFO is clocked with an inverted version of the DFF clock. The FIFO is read at the clock rate of the ethernet core. We developed a Packetization and Control Module (PCM) to combine the data from the FIFO and a Random Access Memory (RAM) to form a User Datagram Protocol (UDP) ethernet packet. The RAM consists of information pertaining to the UDP header bytes. The PCM also distributes the Start of Frame (SoF), End of Frame (EoF) and Source Ready (SRCRDY) signals for the Ethernet module along with the RAM and FIFO Read Enable Signals. The packet description is as follows: Bytes 1–42 correspond to the Ipv4/UDP headers, bytes 43–46 indicate the number of 1PPS signals since the start of the observations, bytes 47–50 represent the packet counts, and bytes >50 are the raw data. A Python-based script is used to start the recording of the data. The data are captured in a standard network file format (pcap) using open source capture format TCPDUMP.[7] The data recording computers are synchronized to the GPS time. The start time is set by the user. Once this time has elapsed, the data recording is triggered and goes on for a pre-set observation period.

APPENDIX C
DATA PROCESSING

Due to the independent recording scheme, data from Stations 1 and 2 should be analyzed offline. The first stage of the analysis is to time-align the data from the data recorders corresponding to the two stations. Initial processing of the data to match the packet counts on both recorders is done using a program written in C language. The count-matched values are written in separate binary files. The correlator pipeline, written in MATLAB, uses this binary file to output the interferometer visibilities. The pipeline is an implementation of the FX Correlator. It was chosen over the XF correlator, because of the flexibility for RFI excision, which is usually a major concern at low radio frequencies. The first step of the correlator pipeline is to align the 1PPS signals from the recorders corresponding to Stations 1 and 2. After alignment, a 4096-point fast Fourier

[7] http://www.tcpdump.org

transformation operation yielding ≈1 KHz spectral resolution is performed on the signals. The resultant voltage spectra of both the channels are multiplied and integrated after RFI excision. Since the cross-correlation is performed offline, the spectral and temporal resolutions are limited primarily by the processing power of the computer on which the correlator is implemented. While analyzing the observed data, we selected an RF bandwidth of ≈100 KHz. The above bandwidth was chosen in order to reduce the coherence loss due to delay errors (Thompson et al. 2004, p. 53). For example, observations of a radio source located at the edge of the FOV of the LBI (≈1°.5 away from the meridian) suffer a maximum decorrelation of only ≈1% with the above bandwidth (see Section 2.1). Note that there are no decorrelation issues during meridian transit observations of radio sources at different declinations with the LBI, since it is oriented in the east–west direction and the observations are limited to ≈±1°.5 around the meridian. The output complex visibilities are in the form of a matrix consisting of M spectral channels × N time channels. They can be further averaged in either time or frequency or both to improve the S/N.

REFERENCES

Arnold, B. C. 2015, Pareto Distributions (Boca Raton, FL: CRC Press)
Bastian, T. S. 2004, P&SS, 52, 1381
Benz, A. O. 1995, in Coronal Magnetic Energy Releases, Vol. 444, ed. A. O. Benz & A. Krüger (Berlin: Springer), 1
Benz, A. O., & Wentzel, D. G. 1981, A&A, 94, 100
Elgarøy, Ø. 1977, Solar Noise Storms (London: Pergamon Press)
Erickson, W. C., Gergely, T. E., Kundu, M. R., & Mahoney, M. J. 1977, SoPh, 54, 57
Hariharan, K., Ramesh, R., Kathiravan, C., Abilash, H. N., & Rajalingam, M. 2016, ApJS, 222, 21
Hudson, H. S. 1991, SoPh, 133, 357
Jacobson, A. R., Massey, R. S., & Erickson, W. C. 1991, AnGeo, 9, 546
Kai, K. 1985, in Solar Radio Physics, ed. D. J. McLean & N. R. Labrum (Cambridge: Cambridge Univ. Press), 415
Kassim, N. E., Lazio, T. J. W., Erickson, W. C., et al. 2007, ApJS, 172, 686
Kassim, N. E., Perley, R. A., Carilli, C. L., Harris, D. E., & Erickson, W. C. 1996, in Cygnus A—Study of a Radio Galaxy, ed. C. L. Carilli & D. E. Harris (Cambridge: Cambridge Univ. Press), 182
Kathiravan, C., Ramesh, R., Indrajit, V. B., & Rajalingam, M. 2011, ApJ, 730, 91
Kathiravan, C., Ramesh, R., & Subramanian, K. R. 2002, ApJL, 567, L93
Kerdraon, A. 1979, A&A, 71, 266
Kishore, P., Kathiravan, C., Ramesh, R., Indrajit, V. B., & Rajalingam, M. 2014, SoPh, 289, 3995
Kishore, P., Ramesh, R., Kathiravan, C., & Rajalingam, M. 2015, SoPh, 290, 2409
Kraus, J. D. 1966, Radio Astronomy (New York: McGraw-Hill)
Krucker, S., & Benz, A. O. 1998, ApJL, 501, L213
Kundu, M. R., & Gopalswamy, N. 1990, SoPh, 129, 133
Malik, R. K., & Mercier, C. 1996, SoPh, 165, 347
Mercier, C., & Chambe, G. 2009, ApJL, 700, L137
Mercier, C., Subramanian, P., Chambe, G., & Janardhan, P. 2015, A&A, 576, A136
Mercier, C., & Trottet, G. 1997, ApJL, 474, L65
Monstein, Ch., Ramesh, R., & Kathiravan, C. 2007, BASI, 35, 473
Nelson, G. J., Sheridan, K. V., & Suzuki, S. 1985, in Solar Radio Physics, ed. D. J. McLean & N. R. Labrum (Cambridge: Cambridge Univ. Press), 113
Parnell, C. E., & Jupp, P. E. 2000, ApJ, 529, 554
Porter, J. G., Fontenla, J. M., & Simnett, G. M. 1995, ApJ, 438, 472
Ramesh, R. 2000, JApA, 21, 237
Ramesh, R. 2005, in Proc. IAU Symp. 226, Coronal and Stellar Mass Ejections, ed. K. P. Dere, J. Wang, & Y. Yan (Cambridge: Cambridge Univ. Press), 83
Ramesh, R. 2011a, in ASI Conf. Ser. 2, First Asia-Pacific Solar Physics Meeting, ed. A. R. Choudhuri & D. Banerjee (Bangalore: ASI), 55
Ramesh, R., Anna Lakshmi, M., Kathiravan, C., Gopalswamy, N., & Umapathy, S. 2012a, ApJ, 752, 107
Ramesh, R., & Ebenezer, E. 2001, ApJL, 558, L141
Ramesh, R., Kathiravan, C., Indrajit, V. B., Beeharry, G. K., & Rajasekara, G. N. 2010, ApJL, 719, L41
Ramesh, R., Kathiravan, C., Indrajit, V. B., & Rajalingam, M. 2012b, ApJ, 744, 165
Ramesh, R., Kathiravan, C., & Satya Narayanan, A. 2011b, ApJ, 734, 39
Ramesh, R., Kathiravan, C., Sundara Rajan, M. S., Indrajit, V. B., & Sastry, Ch. V. 2008, SoPh, 253, 319
Ramesh, R., Nataraj, H. S., Kathiravan, C., & Sastry, Ch. V. 2006, ApJ, 648, 707
Ramesh, R., Sasikumar Raja, K., Kathiravan, C., & Satya Narayanan, A. 2013, ApJ, 762, 89
Ramesh, R., Subramanian, K. R., & Sastry, Ch. V. 1999, SoPh, 185, 77
Sasikumar Raja, K., Ramesh, R., Hariharan, K., Kathiravan, C., & Wang, T. J. 2014, ApJ, 796, 56
Sastry, Ch. V. 1994, SoPh, 150, 285
Steinberg, J. L., Caroubalos, C., & Bougeret, J. L. 1974, A&A, 37, 109
Subramanian, K. R., Gopalswamy, N., & Sastry, Ch. V. 1993, SoPh, 143, 301
Subramanian, P., & Becker, P. A. 2004, SoPh, 225, 91
Subramanian, P., & Cairns, I. H. 2011, JGR, 116, A03104
Suzuki, S., & Dulk, G. A. 1985, in Solar Radio Physics, ed. D. J. McLean & N. R. Labrum (Cambridge: Cambridge Univ. Press), 289
Thejappa, G. 1991, SoPh, 132, 173
Thejappa, G., Gopalswamy, N., & Kundu, M. R. 1990, SoPh, 127, 165
Thompson, A. R., Moran, J. M., & Swenson, G. W., Jr 2004, Interferometry and Synthesis in Radio Astronomy (Weinheim: Wiley-VCH)